Synthesis of uniformly dispersed Fe_2TiO_5 nanodisks: a sensitive photoelectrochemical sensor for glucose monitoring in human blood serum†

Wenbo Lu, *[a] Rui Zhang,[a] Xue Zhang,[a] Yufen Shi,[a] Yupeng Wang[a] and Huanhuan Shi*[b]

A novel photoelectrochemical (PEC) sensor was constructed, using Fe_2TiO_5 nanodisks under visible-light irradiation, for the determination of glucose in human blood serum. The uniformly dispersed Fe_2TiO_5 nanodisks were synthesized for the first time by an ion exchange method and subsequent heat treatment. As excellent catalysts, the Fe_2TiO_5 nanodisks can directly catalyze the oxidation of glucose to produce current in the absence of glucose oxidase. Compared with commercial TiO_2, the Fe_2TiO_5 nanodisks exhibit better activity in the electrocatalytic oxidation of glucose and can generate a photocurrent as a signal for glucose detection. The PEC sensor shows a wide linear range (4 μM–10 mM), a low limit of detection (0.588 μM) and a super sensitivity of 2653 μA mM^{-1} cm^{-2}, which are much better than similar configurations reported previously. This PEC sensor has been successfully used to monitor glucose in human blood serum. Moreover, this PEC glucose sensor based on Fe_2TiO_5 nanodisks possesses great potential for application in point-of-care clinical diagnosis.

1. Introduction

According to a report by the International Diabetes Federation, 537 million people were threatened with diabetes in 2021. By 2045, the number of diabetes patients will increase to 783 million, an increase of 46%. More than 1.2 million children and adolescents are living with type 1 diabetes. At present, diabetes has become a global public health problem.[1,2] The fasting blood glucose concentration of normal subjects is maintained between 3.9 and 6.1 mmol L^{-1}.[3] Blood glucose levels provide important indicators for the diagnosis and treatment of diabetes.[4] Diabetes is one of the main diseases leading to human disability and death.[5,6] Therefore, it is very important to use glucose biosensors and other sensing devices to effectively monitor the glucose concentration in human serum.[7] To develop fast, sensitive and low-cost glucose sensors, many detection methods have developed rapidly in the past few decades. Compared with other detection methods, photoelectrochemical (PEC) technology is quite promising with high sensitivity, low price and easy miniaturization.[8–10] PEC glucose sensors are mainly constructed by the photoelectrocatalytic oxidation of glucose. It has great development prospects because of many intrinsic advantages: (1) PEC analysis has high sensitivity due to the divided excitation source of light and the detection signal of electrochemistry. (2) Compared with the electrocatalytic oxidation of glucose, the PEC procedure can cut down the overpotential of anodic oxidation by the induction of photon energy. (3) The fabrication cost of the PEC sensor is lower than that of electrochemical sensors with noble metal catalysts.

The photoactive materials for the oxidation of glucose, as a photoanode, play an important role in the construction of PEC sensors.[11] The most common photoanodes studied in PEC glucose sensors are made of titanium dioxide (TiO_2) and its composites, which have outstanding properties such as large specific surface area, good chemical stability, non-toxicity and easy preparation.[12–15] Lin's group successfully fabricated three-dimensional flexible Au nanoparticles-decorated TiO_2 nanotube arrays for the efficient PEC sensing of glucose, exhibiting a sensitivity of 21.8 μA mM^{-1} cm^{-2}.[16] Guo *et al.* reported a photoelectrochemical sensing platform based on Au nanorods-decorated TiO_2 nanocomposites for the detection of glucose. The PEC sensor showed a detection limit of 1 μM and a sensitivity of 812 μA mM^{-1} cm^{-2}.[17] While the photoanodes based

[a]*Key Laboratory of Magnetic Molecules and Magnetic Information Materials (Ministry of Education), School of Chemistry and Material Science, Shanxi Normal University, Taiyuan 030031, China. E mail: luwb@sxnu.edu.cn*
[b]*Institut für Quanten Materialien und Technologien, Karlsruher Institut für Technologie, Hermann v. Helmholtz Platz 1, 76344 Eggenstein Leopoldshafen, Germany. E mail: huanhuan.shi@kit.edu*

on TiO_2 composites possess good glucose sensing activity, the PEC sensor can only be effectively excited under ultraviolet light with a wavelength less than 365 nm,[18,19] which is a major defect in its practical application.

As reported, the metal doping of TiO_2 can improve the transport of photogenerated carriers. The light absorption of M′-doped TiO_2 (M′ = Fe, Co, Ni, Cu, Cr, V and Ce) materials is enhanced in the visible light range.[20] It is known that iron titanate (Fe_2TiO_5), a stoichiometric hybrid of Fe_2O_3 and TiO_2, consists of an orthogonal lattice of earth-rich elements,[21] with two cations located in different octahedral positions.[22] Fe_2TiO_5 is an n-type semiconductor with a narrow band gap of about 1.9–2.1 eV,[23–25] which is considered as a promising artificial photocatalyst for photosynthesis. Fe_2TiO_5 is an inorganic photocatalyst with the advantages of high efficiency, simple operation, good repeatability and easy operation.[26,27] Recently, Li's group synthesized three-dimensional porous TiO_2/Fe_2TiO_5/Fe_2O_3 composites for photoelectrochemical water splitting. Fe_2TiO_5 and its related composites have been widely used in photoelectrochemical water splitting, photocatalytic degradation, NO_3^- reduction reaction, water treatment, solar cells and lithium-ion capacitors.[25–31] However, Fe_2TiO_5 and its related composites are rarely used in the field of analysis and detection, especially as a photoelectrocatalyst for the quantitative detection of glucose.

In this study, a PEC sensor was constructed using Fe_2TiO_5 nanodisks under visible light irradiation for application in glucose detection in human blood serum for the first time. The corresponding electron transfer mechanism and sensing mechanism are specialized research. Fe_2TiO_5 nanodisks can directly catalyze the oxidation of glucose to produce a current in the absence of glucose oxidase. As an electron donor, glucose is vulnerable to oxidation to gluconolactone by Fe_2TiO_5 holes, generating a tremendous anodic photocurrent. Compared with commercial TiO_2, the Fe_2TiO_5 nanodisks exhibit better activity in the electrocatalytic oxidation of glucose, which can generate a photocurrent as a signal of glucose detection. The PEC sensor based on Fe_2TiO_5 nanodisks shows a wide linear range, a low limit of detection and super sensitivity. This PEC sensor was also successfully used to monitor glucose with good accuracy in human blood serum. The PEC sensor has great potential for application in monitoring glucose levels in clinical practice.

2. Experimental

2.1. Apparatus

The surface morphology, microstructure and crystal structure of the prepared Fe_2TiO_5 nanostructures were investigated by X-ray diffraction (XRD), scanning electron microscopy (SEM), transmission electron microscopy (TEM), and high-resolution transmission electron microscopy (HRTEM). XRD patterns were obtained on an Ultima IV-185 Advance X-ray diffractometer; the data were recorded in the 2θ range of 10–80°. SEM images were obtained on a JSM-7500F, SEM at an accelerating voltage of 10 kV. TEM and HRTEM images were obtained using a JEM-2100, microscope at an accelerating voltage of 200 kV. X-ray photoelectron spectroscopy (XPS) measurements were conducted on a K-Alpha X-ray photoelectron spectrometer system equipped with an Al X-ray source (1486.6 eV). The compositions and chemical valence states were examined using energy-dispersive X-ray spectroscopy (EDS). Ultraviolet visible diffuse reflectance spectra (DRS) of the samples were recorded with a PERSEE TU-1950 UV-vis spectrometer. The ultraviolet-visible (UV-vis) absorption spectra were obtained in the wavelength range of 400–800 nm. Fourier transform infrared (FT-IR) spectra were recorded between 400 cm^{-1} and 3000 cm^{-1} using a Thermo Nicolet-6700 with KBr as a reference. The photocurrent measurements were conducted on a CHI660E electrochemical workstation. The Fe_2TiO_5 was irradiated using an HGILD30 irradiation source.

2.2. Preparation of MIL-125 (Ti) nanodisks

MIL-125 (Ti) nanodisks were prepared using known methods with a little modification.[32] A certain amount of terephthalic acid was simply dissolved in a DMF : methanol (9 : 1) solution, and then titanium isopropoxide was added dropwise to the solution. After sufficient stirring, the solution was transferred to a stainless-steel autoclave and kept for a time. After cooling naturally, the product was collected by centrifugation, washed with absolute ethanol and ultrapure water, and then dried at 65 °C.

2.3. Preparation of Fe–Ti–O nanodisks

Fe element was doped into MIL-125 (Ti) nanodisks to form Fe–Ti–O nanodisks. To obtain a better Fe–Ti–O nanodisk, we creatively added a surfactant (polyvinylpyrrolidone) to protect the morphology of the Fe–Ti–O nanodisk. In detail, a certain amount of MIL-125(Ti) and polyvinylpyrrolidone was dissolved in ultrapure water, then an aqueous Fe salt solution was added dropwise at 75 °C for 1 h under water bath conditions. The obtained orange precipitate was washed with ethanol and ultrapure water several times and dried in a vacuum at 70 °C.

2.4. Fabrication of the Fe_2TiO_5/ITO electrode

The dried intermediate was calcined for 2 h at the specified temperature, with a heating rate of 2 °C min^{-1}. Then, 5 mg of Fe_2TiO_5 was completely dissolved in 20 μL ultrapure water and 20 μL 0.5% Nafion, and 1 μL configured material was dropped on the ITO.

2.5. PEC detection

PEC detection was conducted in a NaOH solution (pH = 12) at room temperature. The photocurrent was determined from the photocurrent-time curve on an electrochemical workstation (CHI 660E, Shanghai Chenhua). The photoelectrochemical catalyst was assembled with a modified electrode (working electrode), Pt wire electrode (counter electrode), and Ag/AgCl electrode (reference electrode) (KCl saturated). An HGILD30 (Perfect Light, Beijing) was used as an irradiation source in PEC tests and was switched on and off every 30 s.

3. Results and discussion

3.1. Characterization of the synthesized Fe_2TiO_5 nanodisks

The XRD pattern of the synthesized Fe_2TiO_5 can be indexed to the pure Fe_2TiO_5 phase (JCPDS card no. 41-1432). XRD analysis was further conducted to confirm the crystal phase and structural information. As shown in Fig. 1A, the pattern implies the polycrystalline nature of the synthesized Fe_2TiO_5, corresponding to the (200), (101), and (230) planes of Fe_2TiO_5.[32] The SEM images of the Fe–Ti–O precursor are shown in Fig. S1.† A lot of uniform Fe_2TiO_5 nanodisks were synthesized successfully as shown in Fig. 1B. Fig. 1C shows the highly magnified SEM images of Fe_2TiO_5, which display uniform and well-defined discrete nanodisks morphologies with diameters ranging from 400 to 500 nm. The morphology of the Fe_2TiO_5 was characterized by TEM, which was employed to further explore the detailed structure of Fe_2TiO_5 (Fig. 1D). The TEM mapping images reveal that the Fe, Ti, and O elements were evenly dispersed in the sample, indicating the successful doping of Fe element, as shown in Fig. 1E. Fig. 1F shows the HRTEM images show the clear lattice fringes of Fe_2TiO_5. The average lattice fringes of d = 0.271 nm, 0.346 nm, and 0.491 nm correspond to the (101), (230), and (200) planes of Fe_2TiO_5.[33,34]

To confirm the elemental composition of the Fe_2TiO_5, EDS was also carried out. The results reveal that the Fe_2TiO_5 contained the elements Fe, Ti, and O shown in Fig. S2.† XPS measurements were carried out to investigate the detailed elemental compositions and valence states of Fe_2TiO_5. The surface chemical state is characterized by XPS. As presented in Fig. S3,† the XPS confirmed that Fe_2TiO_5 consisted of Fe 2p, Ti 2p and O 1s. The high-resolution Fe 2p peak in Fig. 1G can be transformed into two peaks located at 710.95 eV and 724.5 eV. The high-resolution Ti peak in Fig. 1H (458.25 eV, 464.07 eV) reveals the existence of Ti $2p_{1/2}$ and Ti $2p_{3/2}$;[24] Fig. 1I shows that the high-resolution O 1s spectrum can be divided into three peaks corresponding to the 529.68 eV, 532.01 eV and 533.47 eV.[35] All these observations demonstrate that the Fe_2TiO_5 nanodisks were successfully prepared.

FT-IR spectra were used to identify the chemical bonds, functional groups and molecular geometry of the Fe–Ti–O precursor and Fe_2TiO_5. Fig. 2A and B exhibit peaks at 480–540 cm^{-1} and 500–617 cm^{-1}, ascribed to the characteristic bands of Fe–O and Ti–O, respectively.[36,37] From the FT-IR spectrum of Fe_2TiO_5 in Fig. 2B, the absorption peak appeared at the range of 600–800 cm^{-1}, belonging to Ti–O–Ti stretching vibrations, corresponding to the iron titanate.[38] The FT-IR spectrum of O C O shows two obvious absorption peaks at 2359 cm^{-1}, which are attributed to the symmetric stretching vibration and the anti-symmetric stretching vibration, respectively. The peaks at 1358 cm^{-1} and in the range of 2800–3000 cm^{-1} can be attributed to C–H vibrational modes. The above observations confirm the formation of the as-prepared Fe_2TiO_5 structure, and these bands play a vital role in the enhancement of photocatalytic activity. At the same time, compared with the FT-IR spectrum of the Fe–Ti–O precursor, Fe_2TiO_5 has fewer disordered functional groups, which makes the material more stable. The optical absorption properties of the samples were assessed *via* UV–visible diffuse reflectance spectroscopy, while the direct band gap values were determined utilizing Tauc plots. In comparison to the UV-visible spectrum of the Ti precursor and TiO_2, Fe_2TiO_5 exhibited pronounced absorption within the wavelength range of 300–500 nm, as illustrated in Fig. 2C. This absorption corresponds to a band gap energy of 2.24 eV, as depicted in Fig. S4,†

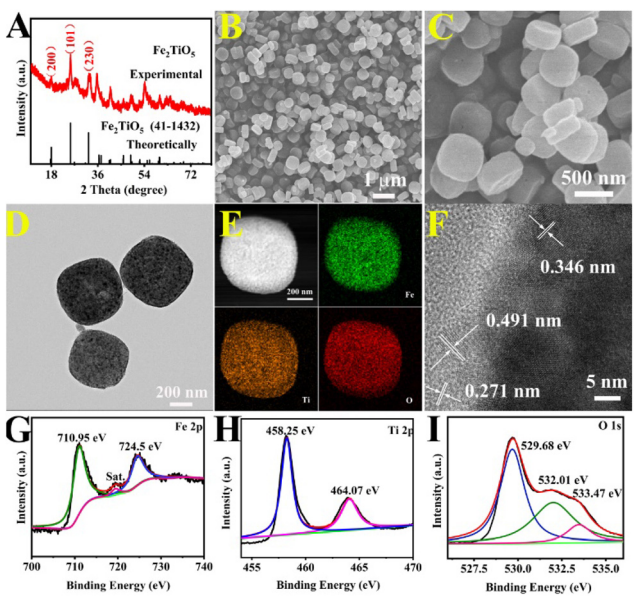

Fig. 1 (A) XRD pattern of the Fe_2TiO_5 nanodisk. (B) and (C) SEM images of Fe_2TiO_5 nanodisks. (D) TEM images of Fe_2TiO_5 nanodisks. (E) The EDX elemental mapping images of Fe, Ti and O elements for the Fe_2TiO_5 nanodisk. (F) HRTEM image of Fe_2TiO_5 nanodisks. High resolution XPS spectra of (G) Fe 2p, (H) Ti 2p, (I) O 1s.

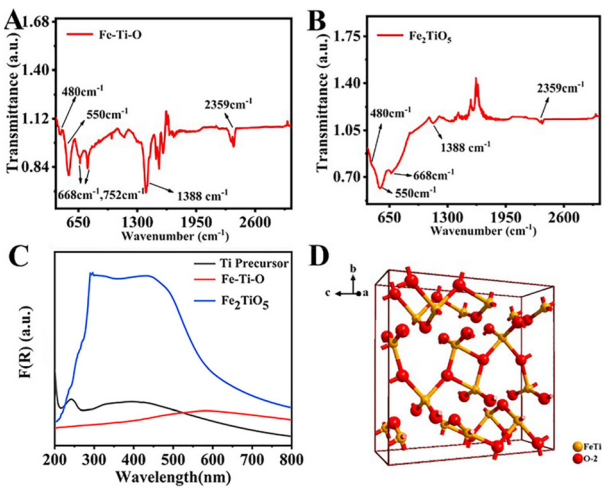

Fig. 2 FT IR spectra of (A) Fe Ti O and (B) Fe_2TiO_5; (C) UV vis DRS spectra of the Ti precursor; Fe Ti O and Fe_2TiO_5 samples. (D) Crystal structure of Fe_2TiO_5; yellow and red spheres represent FeTi and O atoms, respectively.

which signifies that Fe_2TiO_5 possesses the capability to efficiently absorb visible light, a characteristic that is crucial for the successful detection of glucose under visible light conditions. Furthermore, Fig. S5† presents the Mott–Schottky plots for Fe_2TiO_5, with the positive slope in the plot confirming its n-type semiconducting behavior. The Nyquist plots of EIS are presented in Fig. S6.† In the electrochemical impedance spectra obtained for the samples, Z′ and Z″ were the real and imaginary parts of impedance. The bare ITO exhibited a very small R_{et} value (curve e) corresponding to a lower semicircle diameter because of its certain conductivity. As can be seen in Fig. S6,† the Nyquist plots of Fe_2TiO_5 and TiO_2 are comprised of a depressed semicircle in the high- and medium-frequency regions and an inclined line in the low-frequency region. The diameter of the semicircle for the Fe_2TiO_5 sample (7.67 ohms) was much smaller than that of the Ti precursor (23.7 ohms), indicating a lower internal resistance of Fe_2TiO_5. Fe_2TiO_5 (ICSD file No. 35244) has an orthorhombic structure in the space group Cmcm, where two different, octahedral cationic sites, Ti and Fe, are presented in Fig. 2D. Each metal is six-coordinated. The optimized lattice parameters are a = 3.739 Å, b = 9.779 Å, c = 9.978 Å. Crystallographic parameters obtained from riveted refinement are tabulated in Table S1.† From the perspective of theoretical calculation and crystallography, the as-prepared Fe_2TiO_5 nanodisk has an orthorhombic structure with octahedral cationic sites.

3.2. Photoelectrochemical properties of Fe_2TiO_5 nanodisks for glucose detection

The performance of the PEC sensor was studied under visible light as shown in Fig. 3A. The PEC sensor based on Fe_2TiO_5 nanodisks showed a low photocurrent in the absence of glucose but showed an excellent photocurrent in the presence of 1 mM glucose. Fig. 3B exhibits the photocurrents of different electrodes towards 2 mM glucose. The photocurrent intensity of the commercial TiO_2 electrode was 0.63 μA cm^{-2}. The Fe_2TiO_5 nanodisks exhibited a higher photocurrent of 6.43 μA cm^{-2}. The photocurrent intensity of Fe_2TiO_5 nanodisks was around 10.2 times greater than that of the commercial TiO_2 electrode. For comparison, the photocurrent intensities of Fe_2TiO_5 nanodisks were 3.7 and 3.6 times higher than those of the pure Fe–Ti–O and Ti precursor. This can be attributed to the fact that Fe_2TiO_5 has a longer excited state lifetime, which was beneficial to the high charge separation efficiency. The sensitivity of the PEC sensor greatly relies on the pH of the electrolyte. In the pH range of 9 to 13, the PEC sensor based on Fe_2TiO_5 nanodisks exhibited the highest photocurrent intensity at pH = 12, as shown in Fig. 3C. As a result, the optimal pH (pH = 12) was chosen by evaluating different pH values used in the amperometry technique. The amperometry technique was used to assess the photoelectrochemical sensing performance of the Fe_2TiO_5 electrode. As presented in Fig. 3D, the optimum applied potential was investigated in NaOH at pH = 12 in the presence of 2 mM glucose at different potentials from 0.4 to 0.75 V. Since the sensitivity of the PEC sensor greatly relies on its applied potential, 0.75 V was chosen as the optimal potential after evaluating different potentials *via* the amperometry technique.

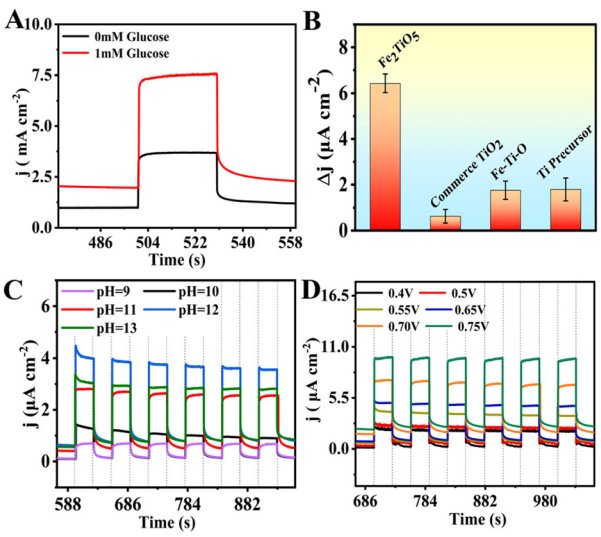

Fig. 3 (A) Photocurrent responses of Fe_2TiO_5 in NaOH (pH = 12) at a potential of 0.75 V. (B) The photocurrent of Fe_2TiO_5, commerce TiO_2, Fe Ti O, and Ti precursor with the addition of 2 mM glucose in NaOH (pH = 12). (C) Photocurrent responses of Fe_2TiO_5 electrode at different pH, ranging from 9 to 13, with the continuous addition of 2 mM glucose. (D) The influence of applied potential on the photocurrent response of the Fe_2TiO_5 electrode towards 2 mM glucose.

3.3. Catalytic performance, selectivity and stability of the PEC sensor based on Fe_2TiO_5 nanodisks

Chronoamperometry is used to determine the performance of Fe_2TiO_5 nanodisks for glucose detection. Fe_2TiO_5 nanodisks can be directly used for the photocatalytic oxidation of glucose in the absence of glucose oxidase. Fig. 4A shows that photocurrent signals at the Fe_2TiO_5 electrode with stepwise increments were received for the successive addition of glucose to pH = 12 NaOH solution every 60 seconds with continuous stirring of the electrolyte solution. The PEC sensor based on Fe_2TiO_5 nanodisks exhibited a linear range of 4 μM to 10 mM with a correlation coefficient of 0.975. The limit of detection (LOD) of the PEC sensor was evaluated to be as low as 5.887 × 10^{-4} mM (S/N = 3). The PEC sensor based on Fe_2TiO_5 nanodisks possessed a super-high sensitivity of 2653 μA mM^{-1} cm^{-2}. The selectivity of the PEC sensor based on Fe_2TiO_5 nanodisks is one of the vital parameters for the evaluation of glucose sensors. The selectivity of the PEC sensor based on Fe_2TiO_5 nanodisks was evaluated against some common small molecules in human serum. As shown in Fig. 4B, the interferents including sucrose, cytosine, thymine, lactose, maltose, and $NaSO_4$ were added to measure the photocurrents of the PEC sensor based on Fe_2TiO_5 nanodisks. The PEC sensor based on Fe_2TiO_5 nanodisks exhibited high photocurrent intensity towards 1 mM glucose. No apparent increases in the photocurrents were observed with the addition of 10 mM interferents. Consequently, the current responses to these interfer-

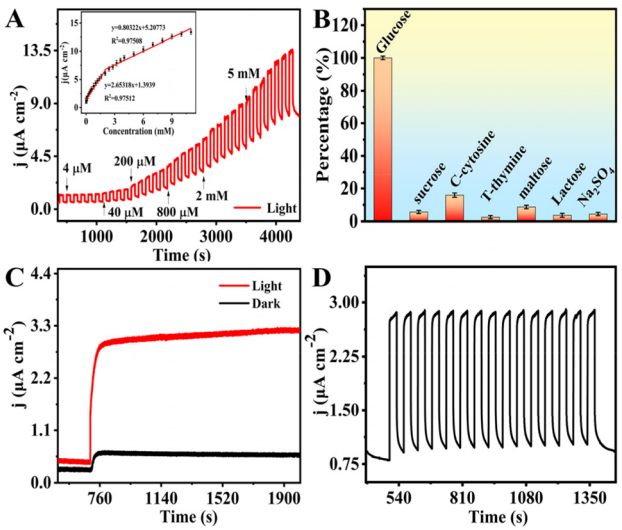

Fig. 4 (A) The photocurrent response of the Fe_2TiO_5 electrode upon the successive addition of glucose NaOH at pH = 12. The inset shows the calibration curve of the photocurrent response *vs.* glucose concen tration. (B) A performance comparison percentage of the Fe_2TiO_5 elec trode with the addition of 1 mM glucose and other interfering species (sucrose, cytosine, thymine, lactose, maltose, $NaSO_4$). (C) Operational stability of the PEC sensor based on Fe_2TiO_5 nanodisks. (D) Photocurrent response of the PEC sensor towards 1 mM glucose with light on and off.

ing species were negligible. This result demonstrates the excellent selectivity of the PEC sensor based on Fe_2TiO_5 nanodisks towards glucose detection.

Stability is another important property of PEC sensors. The stability of the PEC sensor based on Fe_2TiO_5 nanodisks was tested and it remained stable for at least 1000 s as recorded in Fig. 4C. The photocurrent signal showed no obvious change, suggesting that the PEC sensor had good stability. Compared with the dark, the PEC sensor based on Fe_2TiO_5 nanodisks represents higher photocurrent intensity under visible-light irradiation, which remains stable for at least 1000 s. The photo-excitation stability of the sensing platform was first examined by recording the photocurrent density under visible-light irradiation. To further validate the stability of the PEC sensor based on Fe_2TiO_5 nanodisks, the PEC sensor was used to measure the photocurrents toward 1 mM glucose. As illustrated in Fig. 4D, the photocurrent response of the PEC sensor was detected for 15 consecutive cycles, showing little variation and keeping a stable current value. Table S2† shows the comparison of the PEC sensor based on Fe_2TiO_5 nanodisks with other reported sensors for glucose detection. The linear detection range of the PEC sensor based on Fe_2TiO_5 nanodisks was wider than that of other reported sensors based on semiconductor materials. The LOD of the as-prepared PEC sensor was lower than that of other reported sensors. This can be ascribed to Fe_2TiO_5 nanodisks possessing large surface areas and a lot of defective sites. As a result, the PEC sensor based on Fe_2TiO_5 nanodisks for the detection of glucose possesses a higher practical value.

3.4. The PEC detection mechanism of glucose

Compared with the commercial TiO_2 or pristine TiO_2, the PEC performance of Fe_2TiO_5 was significantly enhanced because of the extended light harvesting to the visible-light region and improved charge separation.[22,39] However, the significant enhancement of PEC performances of Fe_2TiO_5 nanodisks should not only possess a low detection limit (0.588 μM) but it should also have a wide linear range (4 μM–10 mM) and high sensitivity (2653 μA mM^{-1} cm^{-2}). Therefore, Fe_2TiO_5 nanodisks have good photoelectric chemical properties. In addition, a new part of our study is the first design of Fe_2TiO_5 nanodisks for photoelectrochemical glucose sensing. The mechanism can be explained as follows:

$$Fe_2TiO_5 + h\nu \rightarrow Fe_2TiO_5^{\bullet} + e^- + h^+$$

$$h^+ + H_2O \rightarrow OH^{\bullet}$$

$$e^- + H_2O \rightarrow O_2^{\bullet -}$$

$$O_2^{\bullet -} + OH^- + \text{glucose} \rightarrow Fe_2TiO_5 + \text{gluconic acid} + e^-$$

It is significant to note that the separation efficiency of electron–hole pairs is significant for the performance of PEC sensing. Under visible-light illumination, photo-generated electrons and holes of Fe_2TiO_5 can be separated quickly and efficiently under the largest built-in electric field, as shown in Fig. 5. Fe_2TiO_5 motivated photo-generated electrons and holes are generated in a narrow-band-gap. Upon absorbing light, Fe_2TiO_5 releases electrons during this process. In this case, the photo-induced electrons and holes of Fe_2TiO_5 are separated and the abundant holes generated in the valence band (VB) of Fe_2TiO_5 will be immediately oxidized. This inter-constituent charge recombination enhances the charge separation in composites, which inhibits the recombination rate of photo-generated electrons and holes in Fe_2TiO_5. Therefore, the addition of glucose molecules could promote higher photocurrent. Given the satisfactory performance of the photocurrent responses and characterization analysis results, it has been proven that the PEC sensor based on Fe_2TiO_5 nanodisks was successfully fabricated.

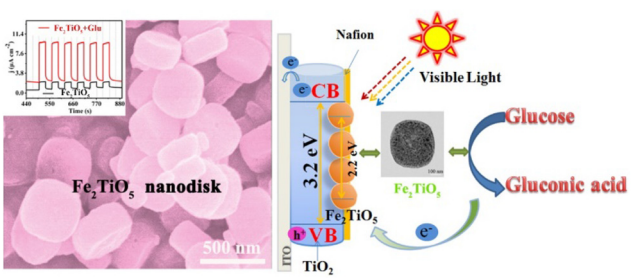

Fig. 5 Schematic illustration of the electron transfer mechanism and target detection of the PEC sensor based on Fe_2TiO_5 nanodisks.

3.5. Real sample analysis

To investigate the practicability of the proposed PEC sensor based on Fe_2TiO_5 nanodisks, the glucose in human blood serum was measured as shown in Fig. 6. This study was conducted in strict accordance with the administrative measures for the clinical laboratories of medical institutions (No. 73, Rev. 2006) issued by the Department of Medical Services Supervision of the Ministry of Health of the People's Republic of China and approved by Shuozhou Modern Hospital (Gubei Street, Shuocheng District, Shuozhou, Shanxi, China). The patients gave consent for the use of the blood in this experiment. This experiment was also supervised and recognized by the Ethics Committee of the Shanxi Normal University. Fig. 6A shows the *i–t* responses of Fe_2TiO_5 nanodisks with the addition of different concentrations of glucose in NaOH (pH = 12) and human blood serum mixed solution. It was observed that the current density can be increased by increasing the glucose concentration. Encouragingly, Fig. 6B shows the regression equation for the data obtained from the PEC sensor based on Fe_2TiO_5 nanodisks, which displays a good positive correlation with a slope of 0.716, an intercept of 3.827, and a correlation coefficient of 0.989. These observations demonstrate that the proposed PEC sensor based on Fe_2TiO_5 nanodisks can be used for the detection of glucose in human blood serum. The recovery test was performed by adding glucose at various concentrations to actual serum samples by the standard addition method. The results are shown in Table 1, with recoveries ranging from 96.7% to 107%, implying the feasibility of the recommended PEC sensor for glucose detection in actual samples.

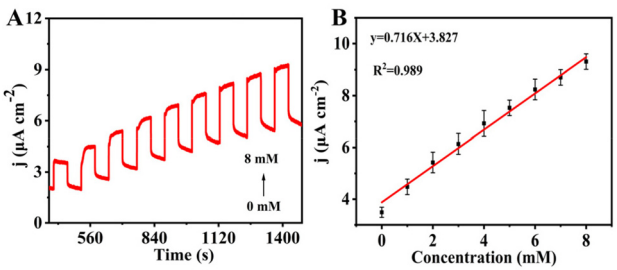

Fig. 6 (A) The *i t* curve of the PEC sensor in NaOH (pH = 12) containing 20% of human blood serum at different glucose concentrations with the light on and off. (B) The corresponding calibration curve of peak currents *vs.* glucose concentration.

Table 1 The detection of glucose in human blood serum using the PEC sensor based on Fe_2TiO_5

Sample	Added (mM)	Found (mM)	Recovery (%)	RSD (%, *n* 3)
1	1.50	1.60	107	3.78
	1.50	1.50	100	
	1.50	1.50	100	
2	3.00	2.93	97.7	2.35
	3.00	3.02	101	
	3.00	3.07	102	
3	4.50	4.57	102	0.630
	4.50	4.57	102	
	4.50	4.62	103	

4. Conclusions

Fe_2TiO_5 nanodisks were prepared using a hydrothermal method and a water bath. We creatively added polyvinylpyrrolidone to protect the morphology of Fe_2TiO_5 nanodisks for the first time. Due to the uniform and topological structure of Fe_2TiO_5 nanodisks, the prepared Fe_2TiO_5 showed high electrocatalytic activity and could serve as a promising electrode material to construct PEC glucose sensors. The PEC sensors based on Fe_2TiO_5 nanodisks can rapidly respond to glucose at the applied potential (+0.75 V) and a super-high sensitivity is easily achieved. The PEC detection mechanism of glucose by Fe_2TiO_5 nanodisks has been explained in detail. In addition, the proposed PEC sensor was successfully applied in the determination of glucose in human blood serum, which is of great significance for providing new and efficient semiconductor materials for glucose detection.

Author contributions

Wenbo Lu: Formal analysis, writing original draft. Methodology, project administration, funding acquisition, supervision. Rui Zhang: Formal analysis, validation, methodology, review & editing. Xue Zhang: Validation, formal analysis. Yufen Shi: Formal analysis, validation, review & editing. Yupeng Wang: Formal analysis, methodology, validation. Huanhuan Shi: Formal analysis, review & editing.

Conflicts of interest

There are no conflicts to declare.

Acknowledgements

This work was supported by the National Natural Science Foundation of China (No. 21705103), the Applied Basic Research Project of Shanxi Province (No. 202103021224251), Scientific and Technological Innovation Projects in Shanxi Universities (No.2019L0460), the Graduate Education Innovation Project of Shanxi Province (2021Y485), and the 1331 Engineering of Shanxi Province.

References

1 Q. Wang, L. Guo, W. Gao, S. Li, L. Hao, Z. Wang, C. Wang and Q. Wu, *Anal. Chim. Acta*, 2022, **1233**, 340511.
2 Y. Wang, Y. Wu and Y. Lei, *Biomater. Sci.*, 2023, **11**, 5727–5757.

3 M. Wei, Y. X. Qiao, H. T. Zhao, J. Li, T. S. Liang, Y. L. Luo, S. Y. Lu, X. F. Shi, W. B. Lu and X. P. Sun, *Chem. Commun.*, 2020, **56**, 14553–14569.

4 J. Zhang, Y. Li, F. Wang, H. Mei and H. Wu, *Sens. Actuators, B*, 2023, **378**, 133206.

5 V. Myndrul, E. Coy, N. Babayevska, V. Zahorodna, V. Balitskyi, I. Baginskiy, O. Gogotsi, M. Bechelany, M. T. Giardi and I. Latsunskyi, *Biosens. Bioelectron.*, 2022, **207**, 114141.

6 Y. Qiao, Q. Liu, S. Y. Lu, G. Chen, S. Gao, W. Lu and X. Sun, *J. Mater. Chem. B*, 2020, **8**, 5411–5415.

7 H. Yang, Y. Hu, X. Yin, J. Huang, C. Qiao, Z. Hu, C. He, D. Huo and C. Hou, *Analyst*, 2023, **148**, 153.

8 Q. Sun, Q. Liu, W. Gao, C. Xing, J. Shen, X. Liu, X. Kong, X. Li, Y. Zhang and Y. Chen, *J. Mater. Chem. A*, 2021, **9**, 26216–26225.

9 A. Qureshi, T. Shaikh and J. H. Niazi, *Analyst*, 2023, **148**, 1633.

10 Y. Wang, Y. Rong, T. Ma, L. Li, X. Li, P. Zhu, S. Zhou, J. Yu and Y. Zhang, *Biosens. Bioelectron.*, 2023, **236**, 115400.

11 X. Zhai, Y. Zhang, Y. Zhang, M. Zhang and J. Tang, *J. Alloys Compd.*, 2023, **939**, 168784.

12 J. J. Tao, H. P. Ma, K. P. Yuan, Y. Gu, J. W. Lian, X. X. Li, W. Huang, M. Nolan, H. L. Lu and D. W. Zhang, *Nanoscale*, 2020, **12**, 7159–7173.

13 S. Y. Fan, X. Y. Li, J. Tan, L. B. Zeng, Z. F. Yin, M. O. Tadé and S. M. Liu, *Appl. Catal., B*, 2018, **227**, 499–511.

14 J. Chen, S. Dai, L. Liu, M. F. Maitz, Y. Liao, J. Cui, A. Zhao, P. Yang, N. Huang and Y. Wang, *Bioact. Mater.*, 2021, **6**, 45–54.

15 Z. L. Li, Z. Q. Li, C. L. Zuo and X. S. Fang, *Adv. Mater.*, 2022, 2109083.

16 X. Zhang, D. Yue, L. Zhang and S. Lin, *J. Mater. Sci. Technol.*, 2020, **56**, 162.

17 L. Guo, Z. Li, K. Marcus, S. Navarro, K. Liang, L. Zhou, P. D. Mani, S. J. Florczyk, K. R. Coffey, N. Orlovskaya, Y. H. Sohn and Y. Yang, *ACS Sens.*, 2017, **2**, 621.

18 B. Chen, L. Liu, K. Liu, F. Tong, S. Wang, D. Fu, J. Gao, J. Jiang, J. Ou, Y. Ye, D. A. Wilson, Y. Tu and F. Peng, *Adv. Funct. Mater.*, 2021, **31**, 2008667.

19 D. Lee, V. U. Baltazar, T. J. Smart, Y. Ping and K. S. Choi, *ACS Appl. Mater. Interfaces*, 2020, **12**, 29275–29284.

20 S. Bibi, S. S. Shah, F. Muhammad, M. Siddiq, L. Kiran, S. A. Aldossari, M. S. S. Mushab and S. Sarwar, *Chemosphere*, 2023, **339**, 139583.

21 L. Wang, N. T. Nguyen, X. J. Huang, P. Schmuki and Y. P. Bi, *Adv. Funct. Mater.*, 2017, **27**, 1703527.

22 W. K. Ho, J. S. Chen and J. J. Wu, *ACS Sustainable Chem. Eng.*, 2021, **9**, 8868–8878.

23 P. S. Bassi, R. P. Antony, P. P. Boix, Y. Fang, J. Barber and L. H. Wong, *Nano Energy*, 2016, **22**, 310–318.

24 C. C. Li, T. Wang, Z. B. Luo, S. S. Liu and J. L. Gong, *Small*, 2016, **12**, 3415–3422.

25 M. M. Zhang, P. P. Liu, H. Tan, H. Z. Zhang, F. Z. Huang, K. Zhang and S. K. Li, *Sci. China Mater.*, 2022, **65**, 124–130.

26 X. L. Lv, K. Q. Nie, H. W. Lan, X. Li, Y. Y. Li, X. H. Sun, J. Zhong and S. T. Lee, *Nano Energy*, 2017, **32**, 526–532.

27 J. J. Deng, X. X. Lv, J. Y. Liu, H. Zhang, K. Q. Nie, C. H. Hong, J. O. Wang, X. H. Sun, J. Zhong and S. T. Lee, *ACS Nano*, 2015, **9**, 5348–5356.

28 Q. Sun and L. M. Qi, *Chem. Eng. J.*, 2021, **426**, 131290.

29 H. Du, H. Guo, K. Wang, X. Du, B. A. Beshiwork, S. Sun, Y. Luo, Q. Liu, T. Li and X. Sun, *Angew. Chem., Int. Ed.*, 2022, **62**, 202215782.

30 E. Elahi, G. Dastgeer, A. S. Siddiqui, S. A. Patil, M. W. Iqbal and P. R. Sharma, *Dalton Trans.*, 2022, **51**, 797.

31 R. Wang, W. Q. Zhu, S. Li, B. B. Zou, L. L. Wang, G. C. Li, X. H. Liu, D. H. L. Ng, J. X. Qiu, Y. Zhao, F. Qiao and J. B. Lian, *Rare Met.*, 2021, **40**, 2424.

32 P. Zhang, X. F. Lu, D. Y. Luan and X. W. Lou, *Angew. Chem., Int. Ed.*, 2020, **59**, 8128–8132.

33 H. Liu, Z. P. Li, H. Y. Sun and Q. F. Lu, *Energy Technol.*, 2020, **8**, 2000215.

34 Z. R. Lou, Y. G. Li, H. Song, Z. Z. Ye and L. P. Zhu, *RSC Adv.*, 2016, **6**, 45343–45348.

35 Y. X. Deng, M. Y. Xing and J. L. Zhang, *Appl. Catal., B*, 2017, **211**, 157–166.

36 K. Bahareh and M. H. Habibi, *J. Ind. Eng. Chem.*, 2019, **80**, 292–300.

37 S. Khanahmadzadeh and S. Salek, *Synth. React. Inorg., Met.-Org., Nano-Met. Chem.*, 2014, **44**, 719–723.

38 E. M. Han, W. D. Yu, L. J. Li, X. Y. Yi, J. Yan and C. Liu, *Chem. Commun.*, 2021, **57**, 2792–2795.

39 Q. H. Liu, J. F. He, T. Yao, Z. H. Sun, W. R. Cheng, S. He, Y. Xie, Y. H. Peng, H. Cheng, Y. F. Sun, Y. Jiang, F. C. Hu, Z. Xie, W. S. Yan, Z. Y. Pan, Z. Y. Wu and S. Q. Wei, *Nat. Commun.*, 2014, **5**, 5122.